



## TIME-DEPENDENT VULNERABILITY ASSESSMENT OF RC BUILDINGS UNDER THE CONSIDERATION OF SSI AND AGING EFFECTS

Stavroula FOTOPOULOU<sup>1</sup>, Sotiria KARAPETROU<sup>2</sup> and Kyriazis PITILAKIS<sup>3</sup>

### ABSTRACT

The present study aims at the investigation of the influence of soil-structure interaction (SSI) and aging in modifying the seismic fragility analysis of reinforced concrete (RC) structures. The consideration of SSI is achieved by applying the direct one-step coupled approach considering both linear elastic and nonlinear soil behavior. A two-step uncoupled approach is also applied to examine the relevant contribution of SSI and site effects on the structural response and fragility. Among the various aging processes, the chloride-induced corrosion is taken into account applying a probabilistic modeling of corrosion initiation time and corrosion rate. Different corrosion aspects are considered in the analysis including the loss of reinforcement cross-sectional area, the degradation of concrete cover and the reduction of steel ultimate deformation. A 9-story RC moment resisting frame (MRF) designed with low seismic code provisions is adopted as a reference structure. Two-dimensional incremental dynamic analysis (IDA) is performed to assess the seismic performance of the initial uncorroded ( $t=0$  years) and corroded ( $t=50$  years) fixed base and SSI structural systems. Time-dependent fragility curves are derived as a function of outcropping peak ground acceleration (PGA) for the immediate occupancy (IO) and collapse prevention (CP) limit states.

### INTRODUCTION

The assessment of seismic vulnerability of RC buildings is a prerequisite for seismic loss estimation and risk management. Currently available seismic fragility databases for RC buildings (SYNER-G Fragility Function Manager, Silva et al, 2013) are developed for fixed-based, as-built structures ignoring SSI and aging effects. However, recent studies (Pitilakis et al., 2014) have shown that these effects might play a crucial role modifying considerably the seismic performance and fragility of RC buildings.

The consideration of SSI is usually achieved by taking into account inertial and kinematic interaction schemes resulting to an elongation of the natural period of the soil-structure system and an increase of system damping due to the energy dissipation at the soil-foundation level compared to the fixed base case (Veletsos and Meek 1974). These effects tend to reduce force demands on the structure. However, because additional translation and rotation effects are introduced to the structure displacement demands may increase (Kramer 1996). SSI and local site effects are generally more pronounced in the case of soft soil formations and high rise structures modifying considerably the free field input motion as well as the dynamic characteristics of the building and finally its response (Stewart et al. 1999). Although there are some studies that take into account the local site effects by

<sup>1</sup> Postdoctoral researcher, Aristotle University, Thessaloniki, sfotopou@civil.auth.gr

<sup>2</sup> PhD student, Aristotle University, Thessaloniki, gkarapet@civil.auth.gr

<sup>3</sup> Professor, Aristotle University, Thessaloniki, kpitilak@civil.auth.gr

providing fragility curves for buildings for different soil conditions (e.g. NIBS 2004), research on the effect of SSI to the expected structure's performance has not received much attention. This may be due to the fact that the incorporation of SSI phenomena in the analysis is generally believed to be beneficial reducing the seismic demand of linear systems. Nevertheless, it has been shown that soil deformability and SSI may modify response and fragility of non-linear structures leading to either beneficial or unfavorable effects depending on the dynamic properties of the soil and the structure as well as the characteristics (frequency content, amplitude, significant duration) of the input motion (e.g. Saez et al. 2011).

Traditionally, the impact of deterioration of the material properties caused by aggressive environmental attack (i.e. aging effect) such as e.g. corrosion, temperature variations, sulphate attack, fatigue, has not been accounted for in the seismic fragility analysis of RC structures. One of the most important environmental degradation mechanisms of RC buildings is corrosion due to chloride penetration, leading to the adverse variation of the mechanical properties of steel and concrete over time (Saetta et al. 2008). Consequently, a reliable evaluation of the seismic structural performance usually requires taking into account degradation mechanisms such as rebar corrosion as they may affect both the safety and serviceability of RC structures, compromising their ability to withstand the loads they are designed for. Recognizing the importance of this issue, several probabilistic models have recently been introduced into the seismic vulnerability assessment framework to assess the time-variant seismic fragility of corroded bridges and RC frame structures (e.g. Ghosh and Padgett 2010, Choe et al. 2009, Yalciner et al. 2012, Pitilakis et al. 2014).

Based on the above considerations, the aim of this study is to further investigate the effect of SSI and aging on the seismic vulnerability of RC buildings. SSI is modeled by applying the direct one-step approach considering both linear elastic and nonlinear soil behavior, while site effects are inherently accounted for. To examine the relative contribution of site and SSI effects, a two-step uncoupled approach is also applied which takes into account site effects on the response of the fixed base structure, but neglects soil-structure interaction effects. Among the various degradation mechanisms, the chloride-induced corrosion is taken into account including different corrosion aspects in the analysis: the loss of reinforcement cross-sectional area, the degradation of concrete cover and the reduction of steel ultimate deformation. A 9-story RC MRF designed with low seismic code provisions is adopted as a reference structure. Fragility curves are derived as a function of PGA for the fixed base (considering or not site effects) and SSI models for the different corrosion scenarios (0, 50 years) based on the statistical exploitation of the results of incremental dynamic analysis of the given structural systems.

## **SELECTION OF THE PROTOTYPE BUILDING MODEL**

The studied building is a nine storey – three bay RC MRF (Kappos et al. 2006) that is considered typical of high rise buildings designed according to the 1959 Greek seismic code ('Royal Decree' of 1959). In the latter regulations, the ductility and the dynamic features of the constructions are completely ignored. Figure 1 illustrates a schematic view of the reference model in the case of fixed base configuration whereas Table 1 presents its main characteristics, namely the total mass, the fundamental period and the strength of concrete and steel.

The numerical modeling of the structure is conducted using OpenSees finite element platform (Mazzoni et al., 2009). Inelastic force-based formulations are employed for the simulation of the nonlinear beam-column frame elements. Distributed material plasticity along the element length is considered based on the fiber approach to represent the cross-sectional behaviour. The modified Kent and Park model (Kent and Park 1971) is used to define the behavior of the concrete fibers, yet different material parameters are adopted for the confined (core) and the unconfined (cover) concrete. The uniaxial 'Concrete01' material is used to construct a uniaxial Kent-Scott-Park concrete material object with degraded linear unloading/reloading stiffness according to the work of Karsan-Jirsa (Karsan and Jirsa 1969) with zero tensile strength. The steel reinforcement is modeled using the uniaxial 'Steel01' material to represent a uniaxial bilinear steel material with kinematic hardening described by a nonlinear evolution equation.

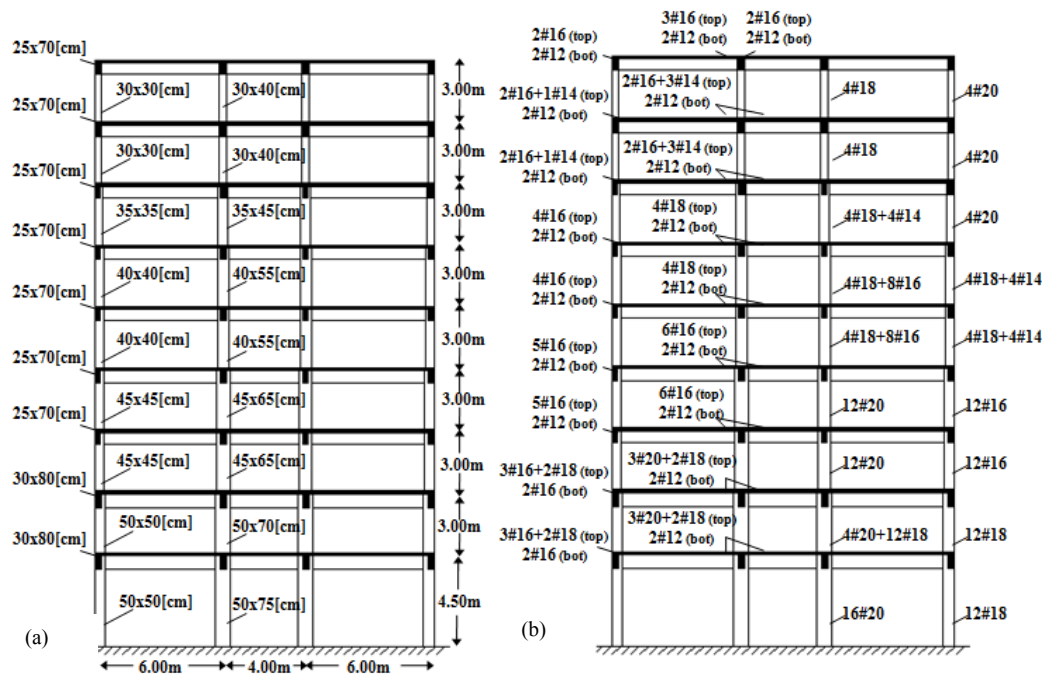


Figure 1. Schematic representation of the geometrical and structural properties of the reference MRF used for the vulnerability assessment: (a) cross sections and (b) reinforcement details

Table 1. Main characteristics of the reference building

Total mass [t]	Initial fundamental period T [sec]	$f_c$ [MPa]	$f_y$ [MPa]
334.0	0.89	14	400

## SOIL-STRUCTURE-INTERACTION MODELING

The consideration of SSI is achieved by applying the direct one-step approach, which accounts simultaneously for inertial and kinematic interaction schemes. The dynamic analyses of the SSI configurations are conducted using OpenSees. The soil is modeled in two-dimensions with two degrees-of-freedom using the four-node plane strain formulation of a bilinear isoparametric quadrilateral ('quad') element. To account for the finite rigidity of the underlying half-space, a Lysmer-Kuhlemeyer (Lysmer and Kuhlemeyer 1969) dashpot is incorporated at the base of the soil profile. The elastic bedrock ( $V_{s,bedrock}=900\text{m/sec}$ ) lies at 30m beneath the ground surface. It is noted that due to the consideration of elastic half-space it was possible to directly apply the outcropping rock motion at the base of the soil model (Kwok et al. 2007). The grid adopted has a total length of 220m with a depth of 30m that includes approximately 6600 four-node quadrilateral elements. The geometry of the mesh allows an adequate number of elements to fit within the wavelength of the chosen shear wave. Considering that the maximum frequency of interest is set to 10Hz we adopted a relatively dense discretization, with quadratic elements of 1.0m x 1.0m.

A first series of analyses is conducted for the fixed base structure (see Figure 1) founded on rock by imposing the outcropping bedrock input motions. To gain further insight into the influence of SSI and site effects on fragility analysis, the SSI effect considering both linear elastic and nonlinear soil behavior is investigated. For the elastic soil profile an average shear wave velocity  $V_{s,30}$  equal to 200m/sec corresponding to ground type C of the Eurocode 8 soil classification system is considered. Soil nonlinearity is introduced using a pressure-independent multi yield surface incremental plasticity model (Yang et al. 2008). We consider a homogenous cohesive soil with an undrained shear strength  $C_u$  equal to 110 KPa underlying the elastic half-space. During the static analysis phase material behavior is linear elastic. In the subsequent dynamic (fast rate) loading phase, the stress-strain

response is turned to elastic-plastic following the multi-surface (nested surfaces) plasticity concept, with an associative flow rule with Von Mises yield surfaces. Since the model considers elastoplastic soil behavior, a considerable amount of hysteretic energy dissipation is represented by the multi-yield function considering that extensive plastic deformation is expected to occur during ground shaking. In this study, a user-defined backbone curve which establishes yield surfaces and plastic shear moduli between yield surfaces is used based on the shear modulus reduction curve provided by Darendeli (2001) for clay soil with plasticity index  $PI=30$  and atmospheric pressure  $p'_0 = 1 \text{ atm}$ .

Additionally, a two-step uncoupled approach is also applied in which, a 1D seismic response analysis of the given (elastic or inelastic) soil profile is first performed and then the obtained free field motion is imposed as input ground motion to the fixed base structural model. It is noted that the 1D soil profile composed of four-node quadrilateral elements used the same vertical discretization as the one used for complete 2D SSI model. This approach takes into account site effects including (or not) soil nonlinearity, but neglects SSI effects. Thus, it allows gaining further insight into the relative contribution of site and SSI effects in fragility analysis. The applied modeling approaches are presented schematically in Figure 2.

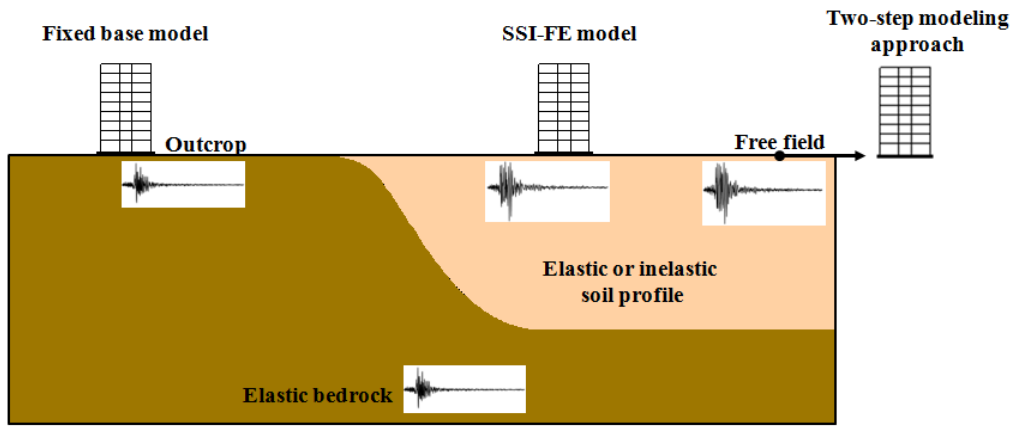


Figure 2. Schematic view of the applied modeling approaches

## CONSIDERATION OF AGING EFFECTS

In this paper, the corrosion of reinforcing bars due to the ingress of chlorides is considered as the aging effect, as it is reportedly one of the most serious and widespread deterioration mechanisms of RC structures. The probabilistic model proposed by FIB- CEB Task Group 5.6 (2006) is adopted to model corrosion initiation time due to chloride ingress that is expressed as:

$$T_{ini} = \left( \frac{\alpha^2}{4 \cdot k_e \cdot k_t \cdot D_{RCM,0} \cdot (t_0)^n} \cdot \left( \text{erf}^{-1} \left( 1 - \frac{C_{crit}}{C_s} \right) \right)^2 \right)^{\left( \frac{1}{1-n} \right)} \quad (1)$$

where  $T_{ini}$ =corrosion initiation time (years) ;  $\alpha$ =cover depth (mm) ;  $C_{crit}$ =critical chloride content expressed as a percentage by weight of cement (wt % cement);  $C_s$  = the equilibrium chloride concentration at the concrete surface expressed as a percentage by weight of cement (wt % cement);  $t_0$ = reference point of time (years);  $D_{RCM,0}$ =Chloride migration Coefficient ( $\text{m}^2/\text{s}$ );  $k_e$ =environmental function;  $k_t$ =transfer variable equal to 0.832;  $\text{erf}$ =Gaussian error function and  $n$ =aging exponent.

The statistical quantification of the model parameters describing the chloride induced corrosion adopted for the present study is given in Table 2 in accordance with FIB- CEB Task Group 5.6 (2006) prescriptions and the available literature (e.g. Choe et al. 2009; Ghosh and Padgett 2010). An atmospheric exposure environment (e.g.  $k_e=0.67$ , Choe et al. 2009) with water-to cement ratio of the concrete material equal to 0.5 is assumed for the considered chloride induced deterioration scenario. It is noted that the adopted corrosion rate implies a relatively high corrosion level (Stewart, 2004). First Order Second Moment (FOSM) reliability analysis is conducted to assess  $T_{ini}$ . Based on the applied probabilistic model, mean value for  $T_{ini}$  is estimated as 7.01 years.

Table 2. Statistical characteristics of parameters affecting the chloride induced corrosion of RC elements adopted in the present study

Parameter	Mean	Coefficient of variation ( <i>cov</i> )	Distribution
Cover Depth (mm) $\alpha$	20	0.40	Lognormal
Environmental function $k_e$	0.67	0.17	Normal
Chloride migration Coefficient ( $D_{RCM,0}$ ) (m <sup>2</sup> /s)	1.58E-11	0.20	Normal
Aging exponent $n$	0.362	$cov=0.677, a=0.0, b=0.98$	Beta
Critical Chloride Concentration ( $C_{crit}$ ) wt % cement	0.6	$cov=0.25, a=0.2, b=2.0$	Beta
Surface Chloride Concentration ( $C_s$ ) wt % cement	1.283	0.20	Normal
Rate of Corrosion ( $i_{corr}$ ) mA/cm <sup>2</sup>	2	0.25	Normal

The effects of corrosion are assumed to be distributed uniformly around the perimeter and along the concrete members. Once the protective passive film around the reinforcement dissolves due to continued chloride ingress, corrosion initiates and the time-dependent loss of reinforcement cross-sectional area can be expressed as (e.g. Ghosh and Padgett 2010):

$$A(t) = \begin{cases} n \cdot D_i^2 \cdot \frac{\pi}{4} & \text{for } t \leq T_{ini} \\ n \cdot (D \cdot (t))^2 \cdot \frac{\pi}{4} & \text{for } t \geq T_{ini} \end{cases} \quad (2)$$

where  $n$ =number of reinforcement bars;  $D_i$ =initial diameter of steel reinforcement;  $t$ =elapsed time in years and  $D(t)$ =reinforcement diameter at the end of  $(t - T_{ini})$  years, which can be defined as:

$$D(t) = D_i - i_{corr} \cdot \kappa \cdot (t - T_{ini}) \quad (3)$$

where  $i_{corr}$ =rate of corrosion (mA/cm<sup>2</sup>);  $\kappa$ =corrosion penetration ( $\mu\text{m}/\text{year}$ ) ( $\kappa=11.6\mu\text{m}/\text{year}$  uniform corrosion penetration for generalized corrosion, Stewart 2004).

Due to the radial pressure developed along the steel bar surfaces, caused by the increasing volume of the corrosion products, the tensile stresses in the concrete surrounding the rebars may exceed the tensile strength leading thus to the cracking of the concrete cover. The cracking and spalling of the cover concrete are taken into account by reducing the concrete cover strength according to the model proposed by Coronelli and Gambarova (2004).

Regarding the effects of corrosion on steel mechanical properties the loss of steel ductility is taken into account through the reduction of steel elongation at maximum load. Thus, the reduction of the steel ultimate deformation  $\varepsilon_{su}$  is calculated based on linear interpolation of the experimental results by Rodriguez and Andrade (2001).

Table 3. Percentages (%) of reinforcement area loss, cover concrete strength and steel ultimate deformation reduction for the 50-year corrosion scenario

	Steel area loss (%)	Cover strength reduction (%)	Steel ultimate deformation reduction (%)
Beam	14	73	28
Column	11	54	22

The distribution of the loss of reinforcement area as well as the reduction in concrete cover strength due to corrosion of the RC elements for the considered corrosion scenario ( $t=50$  years) are calculated as a function of the corrosion rate and the corrosion initiation time variables. Table 3 summarizes the mean percentages (%) of reinforcement area loss, cover concrete strength and steel

ultimate deformation reduction due to corrosion of the studied building within the elapsed time ( $t-T_{ini}$ ). For the purpose of the present study, the mean values of the corrosion modeling parameters are adopted for the analysis of the degraded structural models in OpenSees. Additional details regarding the corrosion modeling approach can be found in Pitilakis et al. (2014).

## SEISMIC INPUT MOTION

We selected a representative set of accelerograms that will subsequently be used for non-linear incremental dynamic analysis and will provide the necessary response statistics for the time-dependent fragility analysis. The selected scenario earthquake consists of a set of 15 real ground motion records obtained from the European Strong-Motion Database (<http://www.isesd.hi.is>) (Table 4). They are all referring to outcrop conditions recorded at sites classified as rock according to EC8 (soil type A) with moment magnitude ( $M_w$ ) and epicentral distance (R) that range between  $5.8 < M_w < 7.2$  and  $0 < R < 45$  km respectively. Outcropping records are selected to avoid uncertainties related to soil effects. Additionally in order to eliminate potential source of bias in structural response, the selection of pulse-like records has been avoided. The primary selection criterion is the average acceleration spectra of the set to be of minimal “epsilon” (Baker and Cornell 2005) at the period range of  $0.00 < T < 2.00$  sec with respect to a reference spectra defined based on the ground motion prediction equation (GMPE) proposed by Ambraseys et al. (1996) corresponding to the median of the  $M_w$  and R selection bin. The optimization procedure is performed by making use of the REXEL software (Iervolino et al. 2010). Figure 3 depicts the mean normalized elastic response spectrum of the records in comparison with the corresponding median predicted spectrum of Ambraseys et al. (1996). As shown in the figure, a good match between the two spectra is achieved.

Table 4. List of records used for the IDA

Earthquake Name	Station ID	Date	$M_w$	R (km)	PGA ( $m/s^2$ )	Waveform code
Friuli	ST20	6/5/1976	6.5	23	3.499	000055xa
Montenegro	ST64	15/4/1979	6.9	21	1.774	000198xa
Montenegro (aftershock)	ST68	24/5/1979	6.2	30	0.667	000234xa
Valnerina	ST225	19/9/1979	5.8	5	1.51	000242xa
Valnerina	ST61	19/9/1979	5.8	22	0.6	000246xa
Campano Lucano	ST93	23/11/1980	6.9	23	1.363	000287xa
Lazio Abruzzo	ST140	7/5/1984	5.9	5	0.985	000365xa
Lazio Abruzzo	ST143	7/5/1984	5.9	22	0.628	000368xa
Golbasi	ST161	5/5/1986	6	29	0.538	000410ya
Golbasi	ST161	6/6/1986	5.8	34	0.167	000412xa
Izmit (aftershock)	ST575	13/9/1999	5.8	15	0.714	001243xa
Mt. Vatnafjoll	ST2483	25/5/1987	6	42	0.131	005271ya
Kozani	ST1320	13/5/1995	6.5	17	1.396	006115ya
South Iceland	ST2497	17/6/2000	6.5	34	0.386	006269xa
Firuzabad	ST3293	20/6/1994	5.9	39	0.216	007158xa

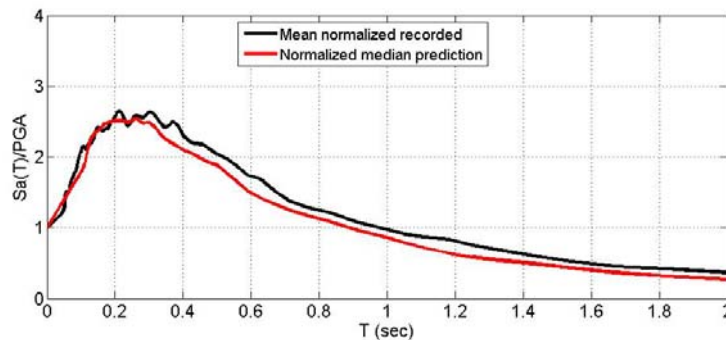


Figure 3. Normalized average elastic response spectrum of the input motions in comparison with the corresponding reference spectrum proposed by Ambraseys et al. (1996)

## INCREMENTAL DYNAMIC ANALYSIS

The IDA procedure is used to determine the seismic performance and finally to assess the time-dependent seismic vulnerability of the given structure under the influence of SSI, site effects and aging. IDA is an emerging analysis method which involves performing a series of nonlinear dynamic analyses under a suite of multiply scaled ground motion records whose intensities should be ideally selected to cover the whole range from elasticity to global dynamic instability (Vamvatsikos and Cornell 2002). IDA curves of the structural response, which provide a relationship between a damage measure quantity (i.e. engineering demand parameter EDP) and a scalable intensity measure (*IM*) of the applied scaled accelerograms, are then constructed by interpolating the resulting EDP-*IM* discrete points.

Within the framework of this study, the damage measure is expressed in terms of maximum interstory drift ratio, maxISD, which is known to relate well to dynamic instability and structural damage of frame buildings. The seismic intensity is described using peak ground acceleration (PGA) recorded on rock outcropping or soil type A according to EC8.

IDA for the fixed base and soil-structure models is conducted by applying the 15 progressively scaled records for the selected time periods  $t=0$  and 50 years. An advanced tracing algorithm, namely the hunt & fill (Vamvatsikos and Cornell 2002; 2004), which ensures that the records are properly scaled with the minimum required computational effort, is used to perform the IDA for the fixed base models. A maximum of 12 runs for each record is allowed while the tracing algorithm was configured to use an initial step of 0.1g, a step increment of 0.01g and a first elastic run designated at 0.005g. Similarly the PGA-stepping algorithm that is used for the models including SSI and site effects to perform the IDA, comprises a first elastic run at 0.005g and an initial step of 0.1. It should be noted that for certain records and time scenarios it was necessary to reduce the step size of the algorithm to increase the accuracy close to the flatline of the IDA curve. To reach the standards of the hunt & fill algorithm the minimum number of converging runs is allowed to vary from 8 to 12 per record depending on the characteristics of the structure and the record itself.

By interpolating the derived pairs of PGA and maxISD for each individual record we get 15 continuous IDA curves for each structural model and time scenario. Figure 4 presents the graphs of the derived IDA curves for each record in terms of PGA and the corresponding summarized across all records IDA curves at 16%, 50% and 84% fractiles for the initial ( $t=0$  years) and corroded ( $t=50$  years) fixed base structure.

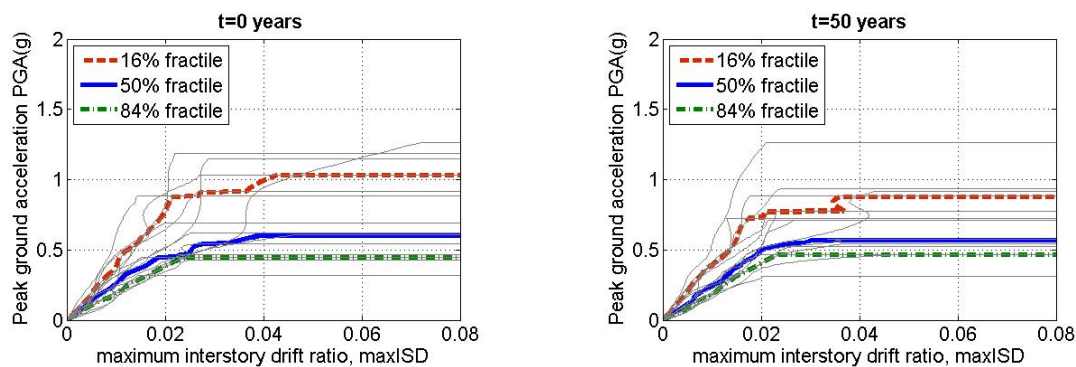


Figure 4. IDA curves for the initial ( $t=0$  years) and corroded ( $t=50$  years) prototype fixed base building model

Next step is the definition of the limit values of the damage states for the derivation of seismic fragility curves. Two limit states are selected in terms of maximum interstory drift ratio, maxISD, representing the immediate occupancy (IO) and collapse, or near collapse prevention (CP) performance levels. The first limit state is defined at 0.5% according to HAZUS prescriptions (NIBS 2004) for RC MRF structures designed with low code seismic provisions, whereas the second is assigned on the median (50%-fractile) IDA curve derived in terms of PGA (see Figure 4). The main idea is to place the CP limit state at a point where the IDA curve is softening towards the flat line but at low enough values of maxISD so that we still trust the structural model (Vamvatsitkos and Cornell 2004). Different CP limit state values are thus chosen on the IDA curve for the structural model

depending on the considered time-dependent corrosion scenario. More specifically a decrease is expected in the CP limit value over time due to corrosion. Thus the CP limit is selected equal to 0.0225 and 0.020 for the for the initial uncorroded ( $t=0$  years) and corroded state of the structure respectively.

## FRAGILITY CURVES

A fragility curve represents a graphical relationship of the probability of exceeding a predefined level of damage (e.g. IO, CP) under a seismic excitation of a given intensity. The results of the IDA (PGA - maxISD values) are used to derive time-dependent (or aging-dependent) fragility curves expressed as two-parameter time-variant lognormal distribution functions. Equation 4 gives the cumulative probability of exceeding a DS conditioned on a measure of the seismic intensity IM.

$$P[DS / IM] = \Phi \left( \frac{\ln(IM) - \ln(\overline{IM}(t))}{\beta(t)} \right) \quad (4)$$

where,  $\Phi$  is the standard normal cumulative distribution function,  $IM$  is the intensity measure of the earthquake expressed in terms of PGA (in units of  $g$ ),  $\overline{IM}(t)$  and  $\beta(t)$  are the median values (in units of  $g$ ) and log-standard deviations respectively of the building fragilities at different points in time along its lifetime and  $DS$  is the damage state. The median PGA values corresponding to the prescribed performance levels are determined based on a regression analysis of the nonlinear IDA results (PGA-maxISD pairs) for each structural model and time scenario ( $t=0$  and 50 years). More specifically, in accordance to previous studies (e.g. Cornell et al. 2002), a linear regression fit of the logarithms of the PGA - maxISD data respectively which minimizes the regression residuals is adopted in all analysis cases. Figure 5 illustrates representative PGA - maxISD relationships for the fixed base structural model founded on rock when outcrop ground motions are imposed for the initial ( $t=0$  years) and corroded ( $t=50$  years) scenario while Figure 6 presents comparative PGA - maxISD diagrams for the initial uncorroded state of the structure considering SSI and fixed base models under linear and nonlinear soil conditions respectively. It is worth noting that while for the linear elastic soil behavior the fixed base model tends to yield higher interstory drift ratios compared to the SSI model for PGA level lower than approximately 0.5g, when soil nonlinearity is considered these results are reversed with the nonlinear SSI model presenting higher drift values for the entire PGA level range.

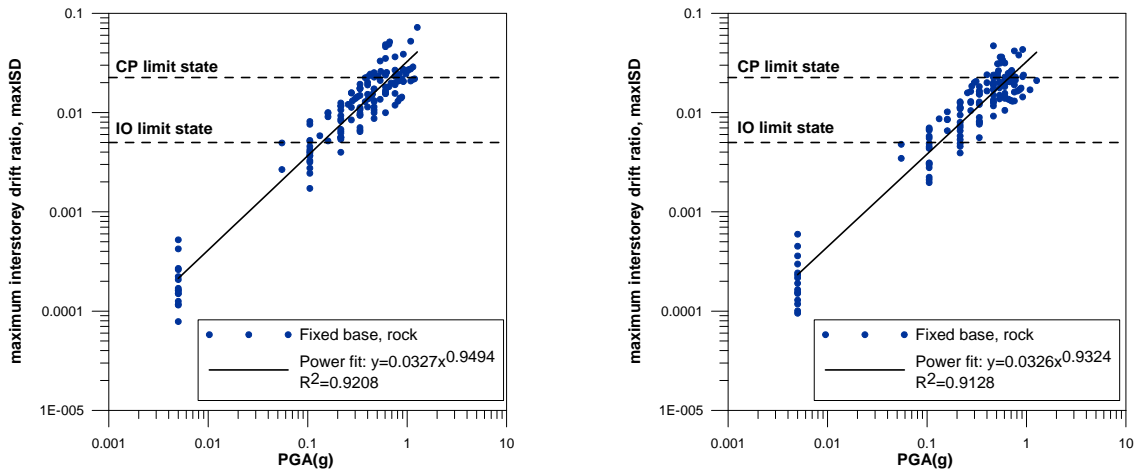


Figure 5. PGA - maxISD relationships for the fixed base model founded on rock for the initial (left) and corroded (right) scenario

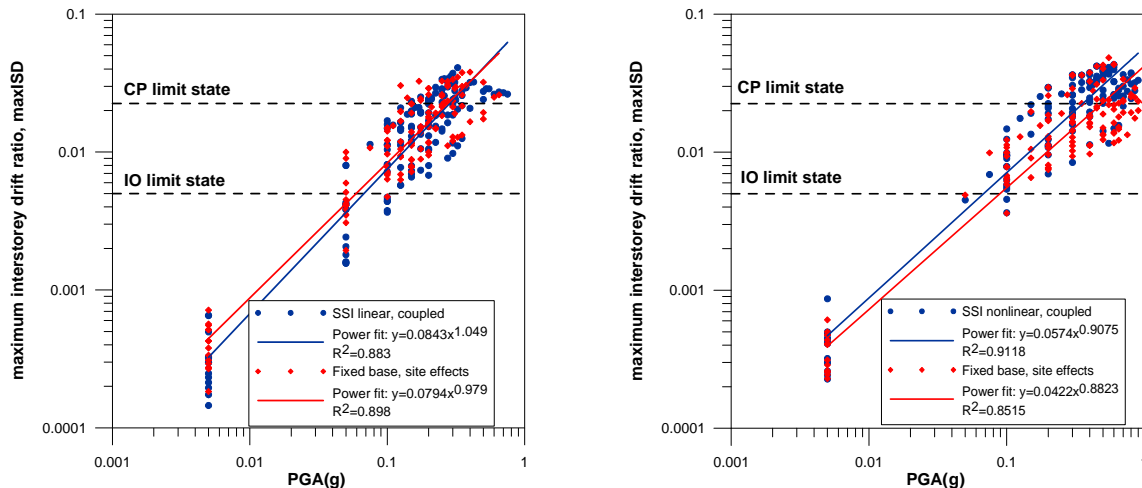


Figure 6. Comparative PGA - maxISD relationships for the SSI and fixed base models under linear (left) and nonlinear (right) soil behaviour for the initial as built state ( $t=0$  years)

The various uncertainties are taken into account through the log-standard deviation parameter  $\beta(t)$ , which describes the total dispersion related to each fragility curve. Three primary sources of uncertainty contribute to the total variability for any given damage state (NIBS 2004), namely the variability associated with the definition of the limit state value, the capacity of each structural type and the seismic demand. The log-standard deviation value in the definition of limit states is assumed to be equal to 0.4 while the corresponding value in the capacity is assumed to be 0.3 for low code structures (NIBS 2004). The third source of uncertainty associated with the demand, is taken into consideration by calculating the dispersion of the logarithms of PGA - maxISD simulated data with respect to the regression fit. Under the assumption that these three log-standard deviation components are statistically independent, the total log-standard deviation is estimated as the root of the sum of the squares of the component dispersions. The herein computed log-standard deviation  $\beta(t)$  values of the curves vary from 0.62 to 0.75 for all structural models and time scenarios.

The derived fragility for the fixed base, uncorroded ( $t=0$  years) structure have been compared with the literature and have been found to be in good agreement verifying the reliability of the proposed fragility functions for the initial as built state. More details regarding the validation results can be found in Pitilakis et al. (2014).

Table 5 presents the lognormal distributed fragility parameters (median and log-standard deviation) in terms of PGA for the initial ( $t=0$  years) and corroded ( $t=50$  years) buildings considering fixed base conditions and SSI configurations. The vulnerability of the structure increases over time due to the corrosion. This increase is generally more noticeable for the CP limit state. In particular, the change in the median PGA values after 50 years is in the order of 7% and 13% for the IO and CP limit states respectively for the fixed base model whereas these percentages are around 14% and 7-22% respectively for the SSI models considering elastic linear or nonlinear soil behavior. Figure 7 illustrates the corresponding graphs of fragility curves for the fixed base structure resting on rock for the initial and corroded scenario. The curves corresponding to the corroded structural state ( $t=50$  years) are shifted to the left in comparison to the initial ones ( $t=0$  years) indicating the increase in vulnerability. Figure 8 depicts the comparative plots of fragility curves for the different SSI configurations compared to the reference fixed base model without modifying the ground motion due to site effects for the considered time scenarios. It is shown that the SSI model, which considers soil nonlinearity is less vulnerable compared to the SSI system where linear elastic soil behaviour is taken into account. This observation is more noticeable for the CP damage limit state and for the initial time scenario ( $t=0$  years). Nevertheless, a significant overall increase of the building's fragility with respect to the fixed base model founded on rock is still shown. Thus, the soil properties and SSI effects may play a crucial role in the expected structural damage, as it is expressed in terms of the maximum interstorey drift ratio, and therefore they should not be neglected for assessment purposes. In Figure 9 we compare the fragility curves for the different coupled SSI cases and fixed base models considering linear elastic and inelastic soil behavior for the initial corrosion scenario ( $t=0$  years).

We observed an important difference between the linear elastic and non-linear case. When soil behavior is assumed linear elastic the coupled approach, where SSI and site effects are considered inherently, has practically no difference with the uncoupled fixed base model where site effects are taken into account. On the other hand, when soil non-linearity is taken into consideration then the coupled case of SSI and site effects lead to a significant increase of the vulnerability compared to the fixed base case where site effects are taken into account through the 1D analysis. A possible explanation is that nonlinear soil behavior introduces additional translation and rotation effects and thus increased displacement demands to the structure.

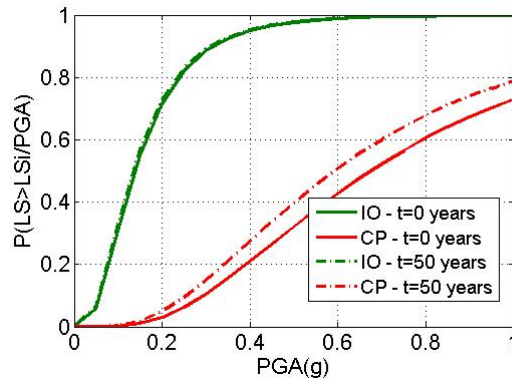


Figure 7. Time-dependent fragility curves corresponding to the initial (t=0 years) and corroded (t=50 years) state of the fixed base model resting on rock

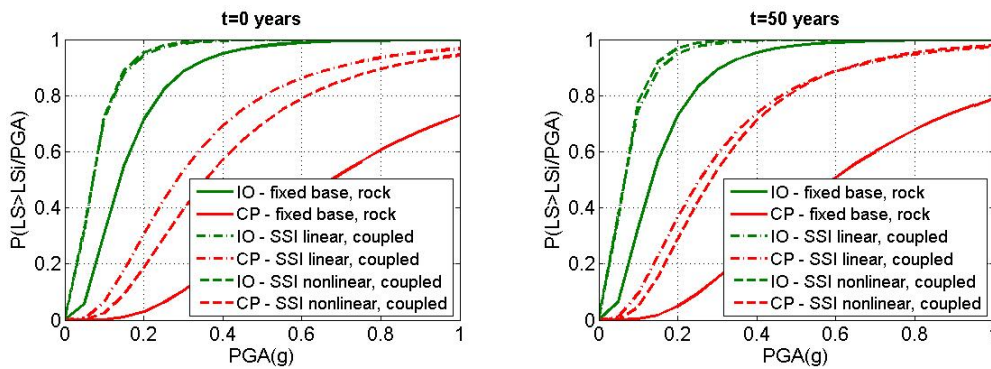


Figure 8. Time-dependent fragility curves for the fixed base structure founded on rock and the SSI structural configurations under linear and nonlinear soil behavior

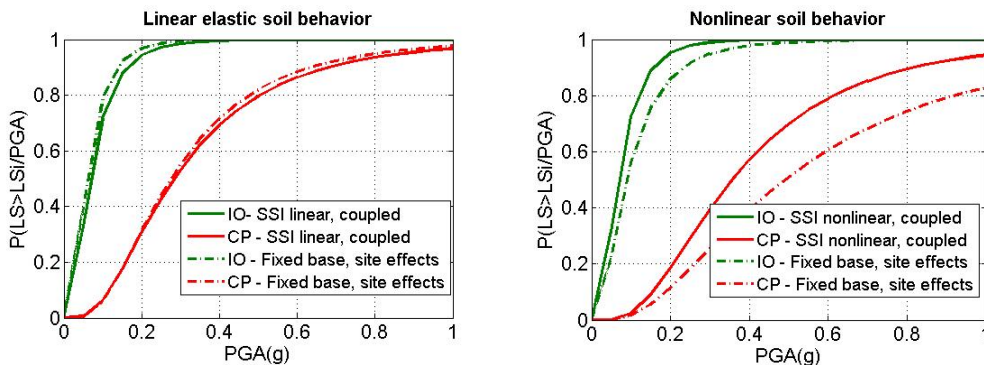


Figure 9. Fragility curves for the fixed base structure considering site effects and the SSI structural configurations under linear (left) and nonlinear (right) soil behavior for the initial as built state (t=0 years)

Table 5. Parameters of the fragility functions in terms of PGA for the considered structural configurations and corrosion scenarios

RC building	Time scenario (years)	Median PGA (g)		Dispersion $\beta(t)$
		IO	CP	
Fixed base, rock	0	0.14	0.68	0.65
	50	0.13	0.59	0.65
SSI linear, coupled	0	0.07	0.28	0.68
	50	0.06	0.26	0.71
SSI nonlinear, coupled	0	0.07	0.36	0.64
	50	0.06	0.28	0.62

## CONCLUSIONS

The seismic vulnerability of a high rise RC frame building designed with low seismic code provisions has been assessed taking into account soil-structure interaction and aging effects due to rebar corrosion. Different corrosion aspects are considered in the analysis including the loss of reinforcement cross-sectional area, the degradation of concrete cover and the reduction of steel ultimate deformation. The consideration of SSI has been achieved by applying the direct one-step uncoupled approach, which accounts simultaneously for inertial and kinematic interaction schemes and eventually the soil non-linear behavior. To gain further insight into the influence of SSI and site effects on fragility analysis both linear elastic and nonlinear soil behavior have been considered. Soil nonlinearity has been introduced through the use of a pressure-independent multi yield surface incremental plasticity model. A two-step uncoupled approach has been also applied which considers the modification of ground motion due to site effects on the response of the fixed base structure. In this way, the importance and relevant contribution of site and SSI effects has been investigated.

IDA was performed for the prototype building model to derive time-dependent probabilistic fragility functions for the IO and CP limit states and different periods in time in terms of PGA. An overall increase in seismic vulnerability over time due to corrosion is shown highlighting the important influence of deterioration due to aging effects on the structural behavior.

The consideration of site and SSI effects may also significantly affect the performance of a RC structure founded on rather soft soil conditions, increasing considerably the vulnerability of the structure compared to the reference case where the structure is supposed as fixed base and no SSI or site effects are taken into account. When soil nonlinearity is introduced these effects are generally expected to be lower for higher levels of seismic loading. When soil behavior is assumed linear elastic the coupled SSI approach has practically no difference with the uncoupled fixed base model where site effects are taken into account. On the other hand, nonlinear SSI leads in an increase of the structure's vulnerability in comparison to the corresponding fixed base model which may be attributed to the complex nonlinear behavior of the underlying soil that may introduce additional translation and rotation effects to the structure yielding to higher displacement demands. Both modeling approaches, however, produce higher vulnerability values compared to the reference fixed base structure founded on rock.

Overall, the present study provides a further insight on the seismic vulnerability of typical RC frame buildings by proposing time-dependent fragility functions applicable to a variety of RC typologies exposed to SSI and aging effects. Validation of the suggested time-dependent fragility curves with field experiments and laboratory tests is certainly warranted to enhance their reliability and to ensure their efficient implementation in seismic vulnerability assessment studies. Given the significance of the SSI and site effects in the structure's vulnerability, future work should also address the investigation of SSI in relation to soil and foundation compliance with different soil conditions.

## ACKNOWLEDGEMENTS

The work reported in this paper was carried out in the framework of the ongoing REAKT (<http://www.reaktproject.eu/>) project, funded by the European Commission, FP7-282862.

## REFERENCES

- Ambraseys NN, Simpson KA, Bommer JJ (1996) "Prediction of horizontal response spectra in Europe," *Earthquake Engineering and Structural Dynamics*, 25: 371-400
- Baker JW, Cornell CA (2005) "A vector valued ground motion intensity measure consisting of spectral acceleration and epsilon," *Earthquake Engineering and Structural Dynamics*, 34:1193-1217.
- CEB-FIB Task Group 5.6 (2006) Model for Service Life Design, fédération internationale du béton (fib).
- Choe DE, Gardoni P, Rosowsky D, Haukaas T (2009) "Seismic fragility estimates for reinforced concrete bridges subject to corrosion," *Structural Safety*, 31: 275-283
- Coronelli D, Gambarova P (2004) "Structural assessment of corroded reinforced concrete beams: modeling guidelines," *Journal of Structural Engineering*, 130(8): 1214-1224
- Darendeli, M. (2001) Development of a new family of normalized modulus reduction and material damping curves, Ph.D. Dissertation, Univ. of Texas
- Ghosh J, Padgett JE (2010) "Aging considerations in the development of time-dependent seismic fragility curves," *Journal of Structural Engineering*, 136(12), 1497-1511
- Iervolino I, Galasso C, Cosenza E (2010) "REXEL: Computer aided record selection for code-based seismic structural analysis," *Bulletin of Earthquake Engineering*, 8:339-362
- Kappos AJ, Panagopoulos G, Panagiotopoulos C, Penelis G (2006) "A hybrid method for the vulnerability assessment of R/C and URM buildings," *Bulletin of Earthquake Engineering*, 4:391-419
- Karsan I, Jirsa J (1969) "Behavior of concrete under compressive loadings," *ASCE J. of the Structural Division*, 95: 2543-2563
- Kent DC, Park R (1971) "Flexural members with confined concrete," *Journal of the Structural Division. Proc. Of the American Society of Civil Engineers*, 97(ST7): 1969-1990.
- Kramer SL (1996) Geotechnical Earthquake Engineering, Prentice-Hall Inc., Upper Saddle River, NJ.
- Kwok AOL, Stewart JP, Hashash YM, Matasovic N, Pyke R, Wang Z, Yang Z (2007) "Use of exact solutions of wave propagation problems to guide implementation of nonlinear seismic ground response analysis procedures," *Journal of Geotechnical Engineering*, 133(11): 1385-1398
- Lysmer J, Kuhlemeyer RL (1969) "Finite dynamic model for infinite media," *Engineering Mechanics*, 95: 859-877
- Mazzoni S, McKenna F, Scott, MH, Fenves GL (2009) "Open System for Earthquake Engineering Simulation User Command-Language Manual," Pacific Earthquake Engineering Research Center, Berkeley, California
- National Institute of Building Sciences (2004) Direct physical damage – General building stock, HAZUS-MH Technical manual, Chapter 5. Federal Emergency Management Agency, Washington, D.C.
- Pitilakis KD, Karapetrou ST, Fotopoulou SD (2014) "Consideration of aging and SSI effects on seismic vulnerability assessment of RC buildings", *Bulletin of Earthquake engineering*, DOI 10.1007/s10518-013-9575-8
- Rodriguez J, Andrade C (2001) CONTECVET – A validated user's manual for assessing the residual service life of concrete structures, GEOCISA, Madrid, Spain
- Saetta A, Simioni P, Berto L, Vitaliani R (2008) "Seismic response of corroded r.c. structures", *International fib Symposium*, Amsterdam, the Netherlands
- Saez E, Lopez-Caballero F, Modaressi-Farahmand-Razavi A (2011) "Effect of the inelastic dynamic soil-structure interaction on the seismic vulnerability assessment," *Structural Safety*, 33: 51-63
- Silva V, Crowley H, Colombi M (2011) Fragility Function Manager, version 2.0, Seventh Framework Program (FP7): SYNER-G: Systemic Seismic Vulnerability and Risk Analysis for Buildings, Lifeline Networks and Infrastructures Safety Gain
- Stewart JP, Fenves GL, Seed RB (1999) "Seismic soil-structure-interaction in buildings I: Analytical aspects," *ASCE Journal of Geotechnical and Geoenvironmental Engineering*, 125(1): 26-37
- Stewart M (2004) "Spatial variability of pitting corrosion and its influence on structural fragility and reliability of RC beams in flexure," *Structural Safety*, 26: 453-470
- Vamvatsikos D and Cornell CA (2002) "Incremental dynamic analysis," *Earthquake Engineering and Structural Dynamics*, 31:491-514
- Vamvatsikos D, Cornell CA (2004) "Applied incremental dynamic analysis", *Earthquake Spectra*, 20(2): 523-553.
- Veletsos AS, Meek JW (1974) "Dynamic behavior of building foundation systems," *Earthquake Engineering and Structural Dynamics*, 3(2): 121-138
- Yalciner H, Sensoy S, Eren O (2012) "Time-dependent seismic performance assessment of a single-degree-of-freedom frame subject to corrosion," *Engineering Failure Analysis*, 19: 109-122
- Yang Z, Lu J and Elgamal A (2008) OpenSees Soil Models and Solid- Fluid Fully Coupled Elements, User's Manual, 2008 ver 1.0, University of California, San Diego